Journal of Structural Geology, Vol. 11, No. 5, pp. 583 to 590, 1989
Printed in Great Britain

0191-8141/89 $03.00 + 0.00

Mylonitic deformation of evaporites in décollements: examples from the Southern Alps, France

J. MALAVIEILLE and J. F. RITZ
Laboratoire de Tectonique, Université des Sciences et Techniques du Languedoc, Place E. Bataillon, 34060 Montpellier Cédex, France

(*Received* 16 *May* 1988; *accepted in revised form* 6 *January* 1989)

Abstract—The ductile deformation of Triassic evaporites is described in two décollements from the Southern Alps of France (the Arc de Nice and Arc de Digne nappes). We show that deformation is not chaotic as is commonly considered: on the contrary it is commonly well organized and is consistent with progressive shearing. Typical shear structures include mylonitic foliation, stretching lineations, folds of various shapes and orientations ('a' type folds and sheath folds), asymmetrical pressure shadows composed of gypsum fibres, shear bands and boudinage. At two sites, lineation directions and analysis of shear criteria allow the kinematics of nappe emplacement to be determined. Computer modelling of pressure shadows allows deformation mechanisms and strain measurements to be determined.

The results of the analysis can be placed in the context of the regional framework of the two décollements. (1) Deformation at the Nice site corresponds to dextral wrenching on a lateral ramp of the décollement along the western limit of the Arc de Nice nappe. Deformation in the ductile fault zone is close to simple shear. (2) Deformation in the second site is associated with a ramp which affects the décollement in front of the Arc de Digne nappe.

The deformation corresponds to shearing towards the southwest, including a pure shear component. This result can be explained by taking into account the effects of the ramp geometry upon the deformation in the décollement. This shows that deformation analysis of evaporites in décollements can be used to understand the mechanisms and kinematics of nappe emplacement.

INTRODUCTION

DUCTILE shearing is commonly described at deep crustal levels, and shear criteria are now classically used in tectonic studies (e.g. Cobbold *et al.* 1987). On the other hand, studies of ductile deformation in décollements at shallow crustal levels are scarce, and associated structures are little known. Until now, only a few studies have described the structures related to the deformation of evaporitic rocks (e.g. in salt, Talbot 1979, Zack & Freund 1980, Larroque & Ansart 1985; in gypsum, Underhill 1988; and in anhydrite from a décollement, Marcoux *et al.* 1987). In the external zones of the Southern French Alps (the Arc de Digne and Arc de Nice nappes) Mesozoic cover rocks are detached from the crystalline basement and décollements are localized in Triassic levels (Goguel 1936, Fallot 1949, Fallot & Faure-Muret 1949, Ginsburg 1959, Graham 1981). Intense shearing occurred within these low strength evaporitic rocks at shallow depths (less than 1000 m, which is the maximum thickness of the cover in this area).

The purpose of this paper is first, to describe the structures associated with this deformation and to show that these structures constitute reliable kinematic indicators. In the second part of the paper, the results of the deformation analysis are discussed and applied to the Alpine regional tectonic framework of the two thrust systems.

GENERAL SETTING

The two studied sites (NS and DS, located in Fig. 1) are situated in the Southern French Alps (Figs. 1a & b), near the southernmost part of the 'Massifs Subalpins' thrust sheets (Debelmas 1979). In this tectonic domain, Mesozoic and Cenozoic cover rocks (Triassic to Lower Oligocene) are detached from the crystalline basement (Argentera-Mercantour external crystalline massifs). The décollement is located in the Upper Triassic gypsiferous clays and evaporites (Gèze 1960). This study concentrates on the deformation of the evaporitic rocks of the décollements from two complementary tectonic contexts: the western lateral limit of the Arc de Nice thrust sheet and the front of the Arc de Digne thrust sheet (Figs. 1b & c).

The tectonic history of the Arc de Nice is divided into two main events (Gèze 1963, Bulard *et al.* 1975). The first Alpine stage corresponds to a compressional deformation which occurred in Oligocene to Aquitanian (early Miocene) time. NE–SW shortening produced NW–SE-trending folds and thrust faults in the Mesozoic cover. The second event corresponds to the Arc de Nice emplacement which occurred in late Miocene to early Pliocene time. Large displacements towards the south were induced by: (i) N–S horizontal compressive push (bulldozer effect, Malavieille 1984) caused by basal thrusting of the external crystalline massifs (Argentera-Mercantour); and (ii) gravitational sliding associated with basement uplift. Towards the front of the structure, the displacement diminishes and the detachment reaches the surface through numerous thrust faults. Recumbent ramp anticlines are associated with thrusting. Along the lateral limits of the nappe, the earlier structures linked to the first phase are strongly reorientated, thus inducing the typical curved geometry of the Arc de Nice.

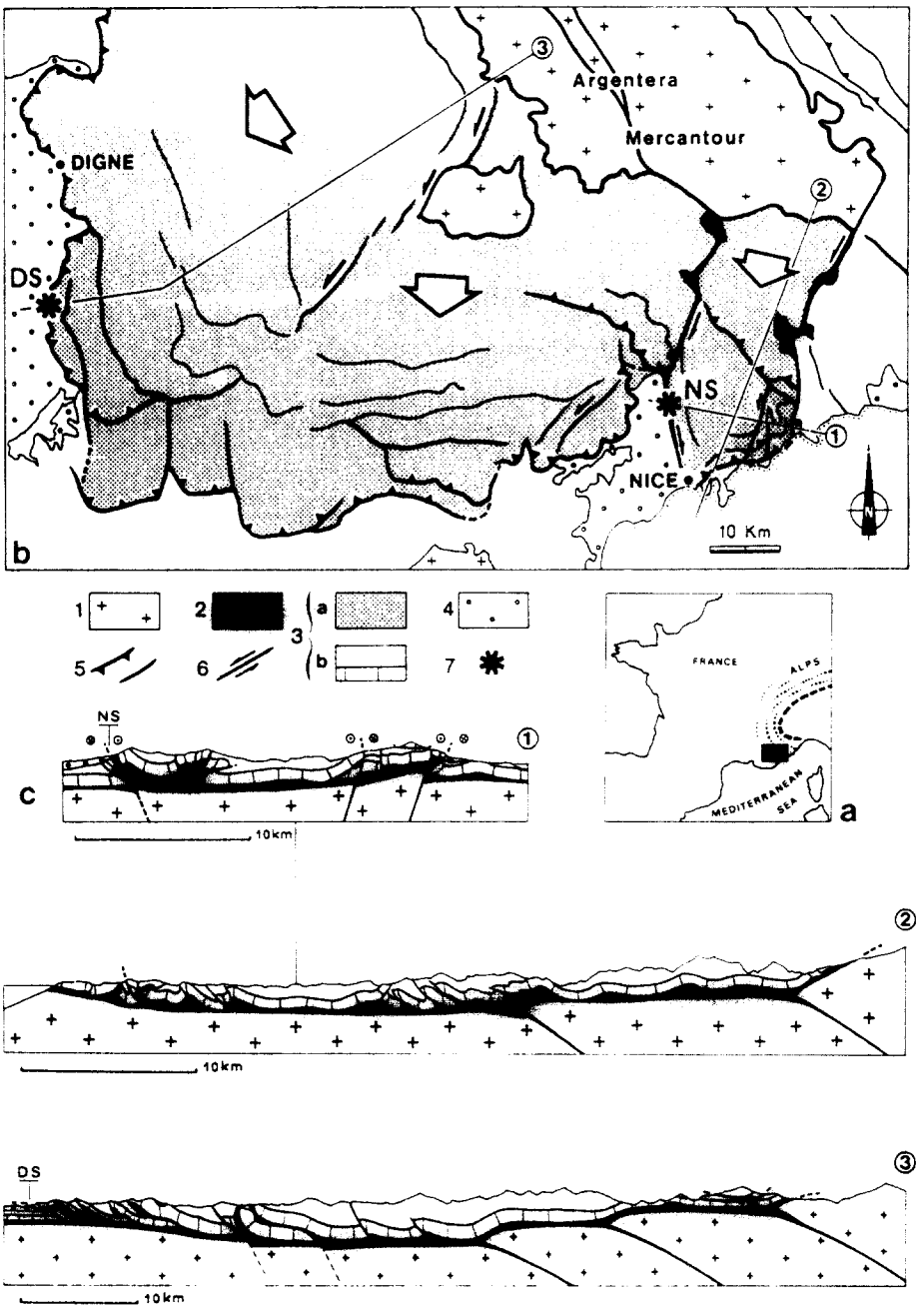

Fig. 1. (a) Location in the Alpine chain. (b) Structural sketch map of the Digne and Nice arcs. 1. Basement, 2. Triassic evaporites of the décollement level. 3a. Mesozoic and Cenozoic rocks of the detached cover (map), 3b. *idem* (cross-sections), 4. Mio-Pliocene deposits, 5. thrust faults, 6. strike-slip faults, 7. location of the two sites studied (NS and DS). (c) Cross-sections (from J. F. Ritz & P. Labaume, unpublished data), located on (b).

Laterally, the thrust system is limited by the two roughly N–S wrench fault zones, the Nice–Vésubie and the Breil–Sospel–Monaco fault systems (Fig. 1b).

Similarly to the Arc de Nice nappe, the Arc de Digne thrust sheet results in the décollement of the Mesozoic units on the Triassic layers (Lemoine 1972, Gigot *et al.* 1974). Folds and thrusts associated with wrench faults indicate NE–SW compression which occurred between the late Oligocene and Pliocene epochs.

DEFORMATION STRUCTURES IN EVAPORITIC ROCKS

The two outcrops (NS and DS on Fig. 1b) show tectonic contacts between Mesozoic limestones, Upper Triassic evaporitic rocks and Pliocene conglomerates. They define a fault zone about 50 m thick. At NS, the deformation associated with wrench movements along the western lateral limit of the Arc de Nice (Fig. 1c, section 1) was studied at an outcrop 2 km north of the village of Castagniers. The fault is oriented N170°E and dips 60°E. DS is situated at the front of the Arc de Digne thrust system (Fig. 1c, section 3) near the village of Saint Jurs. The thrust plane corresponds to a ramp oriented N150°E and dipping 35–40°E. At both sites, the faulted Triassic sequence is mainly composed of gypsiferous-rich clays containing limestone fragments, and the deformation structures are similar.

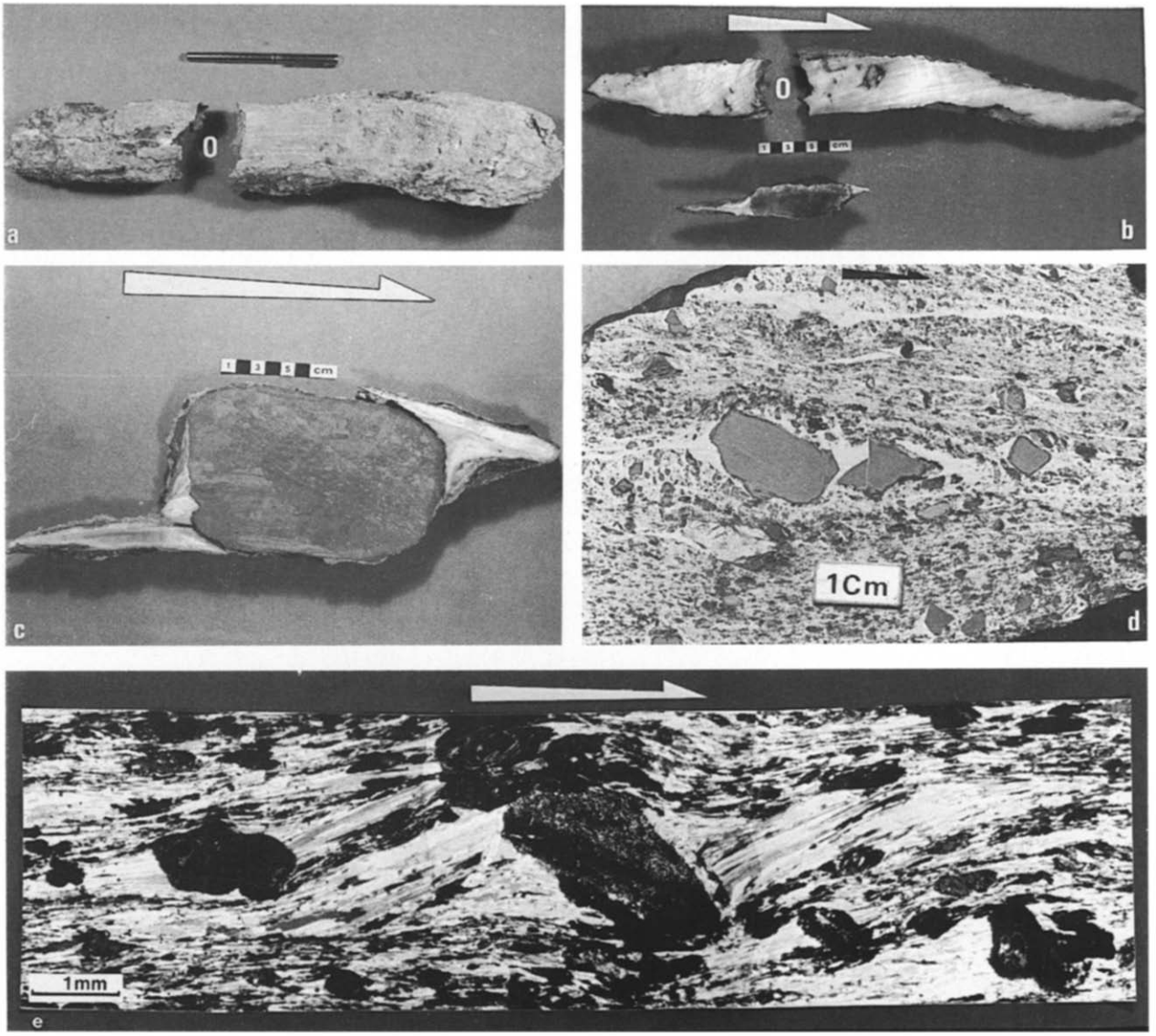

Fig. 2. Pressure shadows (Dignes site): (a) Shape of a decimetric-scale (~50 cm) pressure shadow weathered out of the exposure. The rigid particle (O) has disappeared. (b) Section of same sample showing the asymmetrical organization of gypsum fibres. The second sample (bottom) shows asymmetrical sharp gypsum pressure shadows around a nodule of red anhydrite. (c) Section of a large sandstone pebble showing very asymmetric sharp pressure shadows. (d) Mylonitic foliation in gypsiferous-rich clays from DS ($\lambda_1\lambda_3$ plane). Note the numerous pressure shadows around the clay elements and the synthetic rotation of the two fragments of a stretched object. (e) Asymmetric pressure shadow (polarized light) around a pebble made of argilaceous sandstone (Nice site).

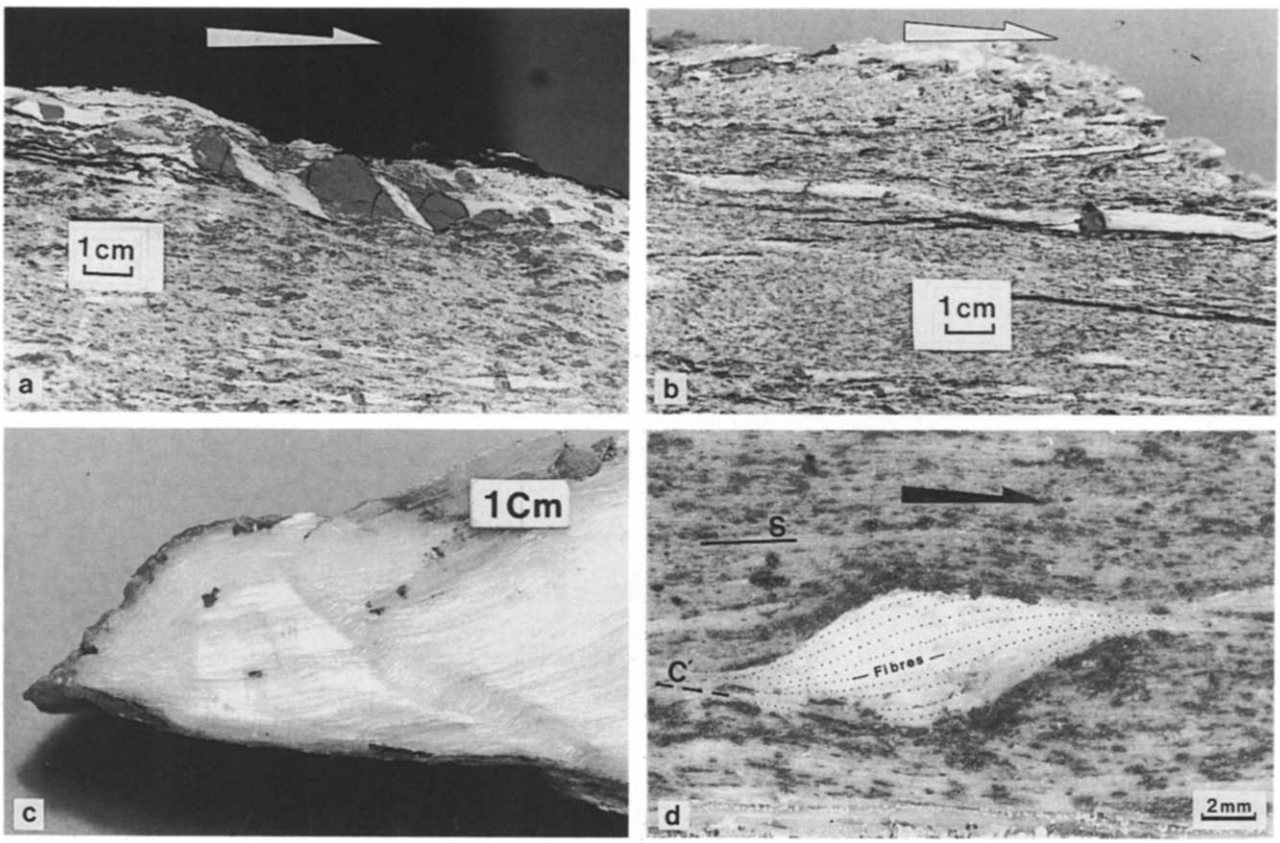

Fig. 3. Boudinage and shear bands. (a) Stretched layer of clay with gypsum fibre growth. Note the back-tilted elements of clay. (b) Boudinage of an elongate pressure shadow associated with the development of shear planes. (c) Pinch structure at the left extremity of the pressure shadow in Fig. 6(b) illustrating the boudinage of elongate pressure shadows. (d) Isolated asymmetric lens-shaped fibre packs associated with shear planes, resulting from pressure-shadow boudinage. (a) and (c) Digne site; (b) and (d) Nice site.

Foliation and lineation

In both fault zones, the initial bedding in the evaporitic rocks has been locally erased by the strong mylonitization (the term mylonitization is used to describe ductile deformation involving grain-size reduction, recrystallization and plastic deformation). The most prominent structural features are the mylonitic foliation parallel to the fault plane and the associated stretching lineation. Lineation directions are N170°E (subhorizontal) at NS, and about N070°E on planes oriented N170° and dipping 40°E at DS, and are defined by syntectonic fibrous gypsum growth in pressure shadows, boudinaged rigid inclusions and elongate nodules of red anhydrite. In places, *C* slickensides and gypsum fibres indicate localized displacement on shear surface. These slickensides are parallel to the ductile stretching of rocks.

In the following analysis, the foliation plane (*S*) is assumed to be the $\lambda_1\lambda_2$ principal plane of the strain ellipsoid and the stretching lineation (*L*) is parallel to the λ_1 axis.

Folds

Numerous folds can be observed ranging from cm- to m-scale. At the DS site, most folds are isoclinal and recumbent, with axes parallel to the lineations. Overturning is mainly towards the SSE, but sometimes towards the NNW, suggesting that the overturning was initiated by the shearing of layers oblique to the shear plane but containing the shear direction (Hugon 1982). They are sometimes refolded by gently reclined folds with the same kinematics suggesting progressive deformation.

Locally, some drag folds have developed in the mylonitic foliation. Their axes are often curved but they are roughly perpendicular to the lineation. The overturning of these folds is consistent with the shear sense determined by other criteria in the fault zone (see the following paragraphs).

Metre-scale sheath folds (Quinquis *et al.* 1978, and in evaporites Marcoux *et al.* 1987, Talbot 1979) have been observed in sections at high angle to *L*, forming eye-like structures.

Pressure shadows, boudinage and shear bands

The most spectacular structures at both sites are the pressure shadows (Fig. 2). They can be found from microscopic-scale (Fig. 2e) to decimetric-scale (the largest pressure shadow, shown in Figs. 2a & b, is more than 50 cm in length). Pressure shadows are of particular interest because they provide information about deformation geometry, local strain magnitude (minimum strain) and shear sense (Choukroune 1971, Malavieille *et al.* 1982, Ramsay & Huber 1983). Most pressure shadows developed around rigid objects in the gypsiferous-rich Triassic clays. Rigid objects are pebbles of Triassic sandstones (Fig. 2c), nodules of red anhydrite (Fig. 2b), isolated elements of stretched and boudinaged

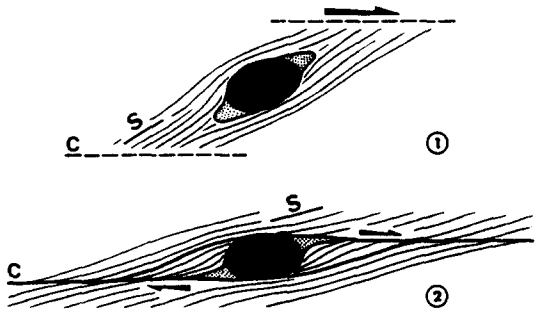

Fig. 4. Sketch showing the development of sharp asymmetrical pressure shadows at the edges of pebbles. Stage 1; pressure-shadow growth (homogeneous deformation under low strain). Stage 2; shear planes (*C*) develop and stop pressure-shadow growth, resulting in a lens-shaped geometry of the foliation (heterogeneous deformation under large strain).

dolomitic (or calcareous) layers, and more commonly fragments of dark clay (Fig. 2d). In the section perpendicular to λ_1, no pressure shadows are visible.

There are two main morphologies. (1) Thin and sharp asymmetrical pressure shadows have developed at the edges of pebbles (Fig. 2c) or elliptical nodules of red anhydrite (Fig. 2b, lower sample). This type of pressure shadow is related to zones of local intense shear and its development seems limited by strain concentration along shear planes, which occurred early during deformation and stopped pressure-shadow growth. This setting results in the formation of a lens-shape geometry of the foliation around the object plus pressure shadow (Fig. 4). (2) Very elongate pressure shadows that are as thick as the object, showing asymmetrical internal orientation of gypsum fibres (Figs. 2b, upper sample, & e). This type develops mainly around fragments of dark clay contained in a gypsiferous-rich matrix. In this case, the homogeneous deformation of the matrix enables the fibres to grow, even under large strains.

There are different kinds of associations between boudinage and shear bands: (i) boudinage of argillaceous layers in which synkinematic interboudin fibre growth shows an antithetic (Fig. 3a) or synthetic (Fig. 2d) rotation of the elements relative to the shear-induced vorticity; (ii) boudinage of thin layers with development of extensional shear bands (Platt & Vissers 1980) without interboudin fibre growth; (iii) pressure-shadow boudinage and related shear bands (Fig. 3b) (these structures will be described in the following paragraph). All these structures indicate a non-coaxial strain history.

PRESSURE-SHADOW SIMULATION AND STRAIN ANALYSIS

In order to determine deformation mechanisms and strain parameters, we have applied the pressure-shadow computer modelling of Etchecopar & Malavieille (1987) to six different natural examples (three from the NS site and three from DS site), which are representative of the deformation observed in the two areas. The results are given in Table 1. The lack of pressure shadows in

Table 1. Results of pressure-shadow analysis. Deformation parameters are as follows. γ_i: size of simple shear increments used for the modelling. γ_f: finite simple shear. K_{i1}: coaxial stretch increment normal to the plane of simple shear. K_{i2}: coaxial stretch increment parallel to the shear plane. K_{f1}: finite coaxial stretch normal to the shear plane. K_{f2}: finite coaxial stretch parallel to the shear plane

Sample	γ_i	γ_f	K_{i1}	K_{i2}	K_{f1}	K_{f2}
NS_1	0.45	6.3	1.0	1.0	1.0	1.0
NS_2	0.45	6.3	0.98	1.02	0.76	1.32
NS_3	0.8	4.8	1.0	1.0	1.0	1.0
DS_1	0.7	10.5	0.87	1.15	0.12	8.07
DS_2	0.80	14.25	0.8	1.25	0.03	28.42
DS_3	0.80	4.8	0.67	1.5	0.09	11.4

sections perpendicular to λ_1 suggests that deformation is close to plane strain. The deformation imposed in the model was therefore plane strain. The best fit between computed and natural pressure shadows is obtained using rigid displacement-controlled fibre models (Etchecopar & Malavieille 1987). Results of these computations are shown in Table 1. Pressure shadows from the Nice site were successfully modelled by deformation close to simple shear. Those from the Digne site, however, required significant components of coaxial deformation in addition to simple shear. These are expressed in Table 1 as stretches $(1 + e)$ normal and parallel to the plane of simple shear. Two results of the computation are illustrated in Figs. 5 and 6(a). Comparison between Figs. 2(b) and 6(a) (sample DS_1) and Figs. 5 and 2(e) (sample NS_1) shows the following discrepancies between the computed and the natural examples. (1) The important differences in length between the two sides of the natural pressure shadow of sample DS_1 can be explained by the shear plane which cuts the fibres at low angle, with associated 'pinch' structure (Fig. 3c) typical of boudinage, at the top left-hand side of the pressure shadow. This suggests that these very elongate pressure shadows can be boudinaged and crosscut by shear bands which displace the stretched pressure shadows elements far away from the object. This phenomenon is common in very elongate pressure shadows (Fig. 3b). (2) In sample NS_1 the sharp terminations of the natural pressure shadow suggests that far away from the object, the fibres can be deformed. Thus, the computed model (Fig. 5) differs slightly from the natural example (Fig. 2e), because the model cannot take into account variations in the behaviour of natural pressure shadows that depend on strain conditions.

These observations raise questions about the maximum possible length of pressure shadows, and hence the maximum strain that can be indicated, in such deformation conditions. It is likely that when large strains occur, rigid pressure shadows are boudinaged and cut by shear bands which therefore limit the length. The mechanism shown in Figs. 6(b) & (c) is responsible for the initiation and development of most of the shear bands and lens-shaped fibre packs (Fig. 3d) in these mylonites. In every case, the values in Table 1 should be considered as minimum strains.

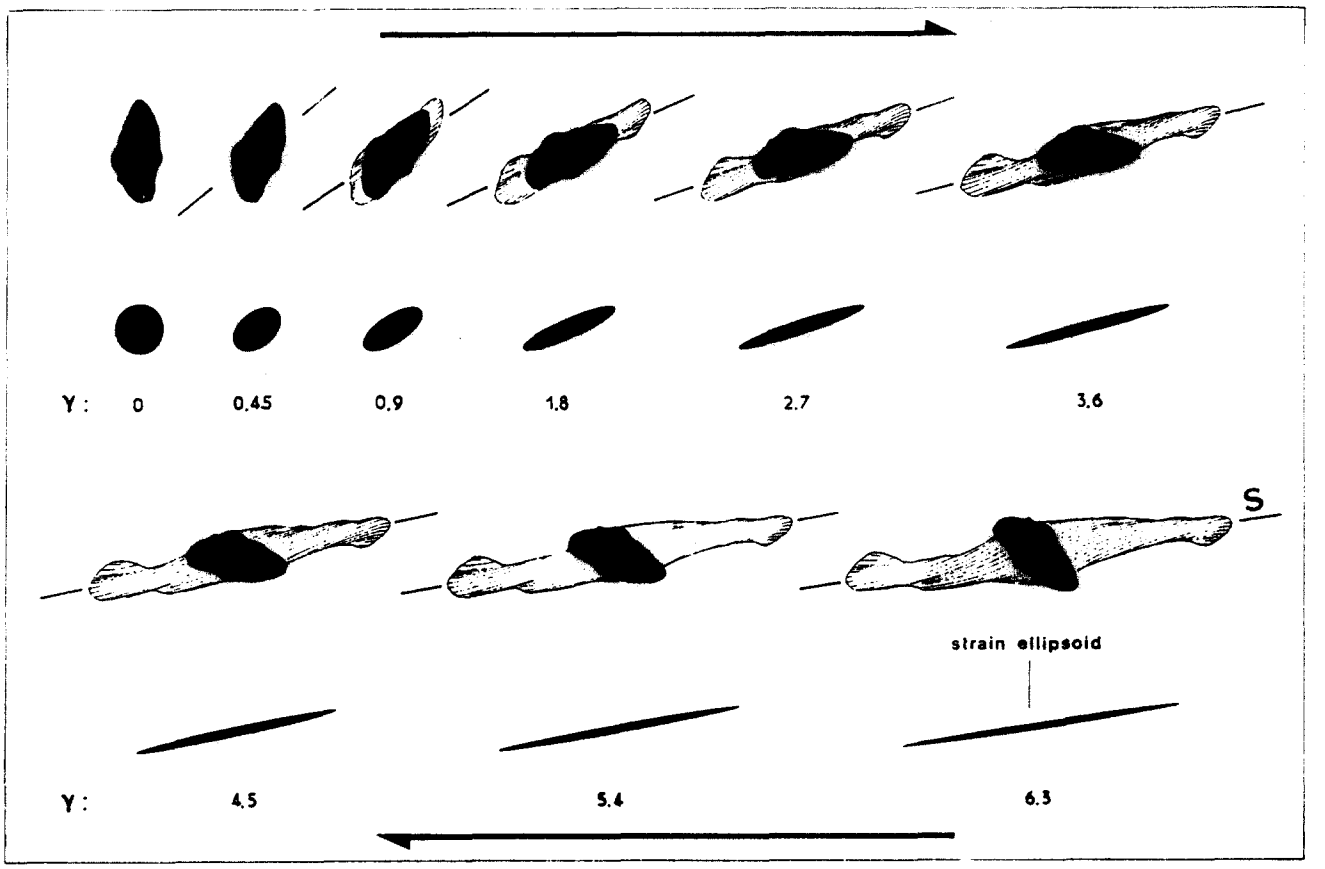

Fig. 5. Computed pressure shadow from example 1. Model parameters are rigid and displacement-controlled fibres (compare the result with the natural sample of Fig. 2e).

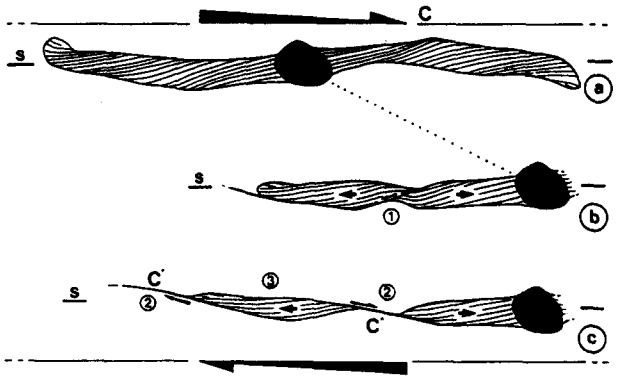

Fig. 6. (a) Computed pressure shadow of example 2 (compare the result with the natural sample of Fig. 2b). (b) and (c) Model proposed to explain the discrepancies between computed and natural pressure shadows. (b) Stretching of elongate pressure shadow induces boudinage (1) during the progressive deformation. (c) Shear planes (2) develop between the stretched elements of the pressure shadow to form isolated lens-shaped fibre packs (3) (see Fig. 3d).

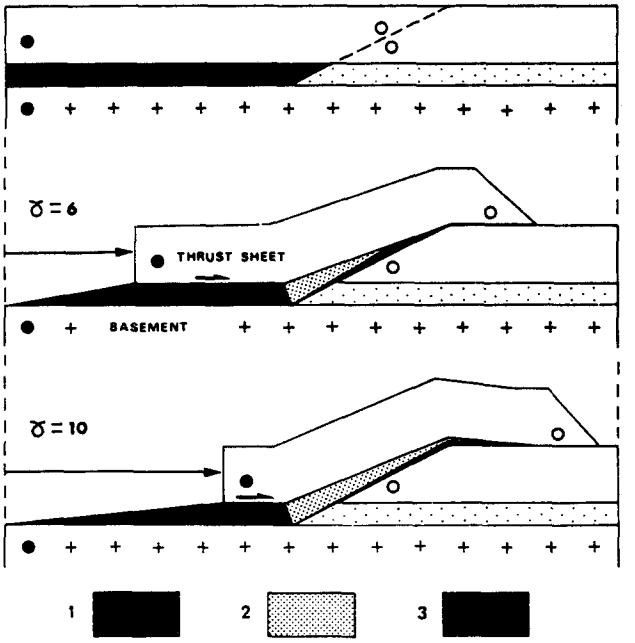

Fig. 7. Sketch showing the effects of a ramp on the deformation in the décollement. (1) Domain which underwent only simple shear; (2) domain which underwent firstly simple shear, secondly a mixed deformation regime (pure shear plus simple shear); (3) domain which underwent only the mixed regime: pure shear plus simple shear.

DISCUSSION—CONCLUSIONS

In this paper, we have described the deformation of evaporitic rocks that constitute the décollement level of two Alpine nappes, and shown that this deformation is consistent with a progressive shearing history.

The observed structures allow determination of the finite strain and kinematics of nappe emplacement, particularly the directions and senses of shearing (or wrenching) on the décollements. At the NS site, the deformation analysis shows a dextral wrenching, indicating that a lateral ramp transforms the differential displacements between the Arc de Nice nappe and the autochthonous Mesozoic and Cenozoic sediments of the foreland. Pressure-shadow analysis suggests that the deformation was close to simple shear.

At the DS site, the deformation analysis shows that in front of the Arc de Digne nappe, thrusting occurred towards the WSW. Computer modelling of pressure shadows suggests that deformation differs significantly from simple shear and that a coaxial component is present.

This last result needs discussion. Two different explanations may be proposed to account for the coaxial component shown at DS. (1) The first explanation involves a possible extension along the λ_2 strain axis (i.e. the strain was not plane) and consequently a lateral flow of evaporitic material; but this does not agree with the observations (no pressure shadows develop in the λ_2–λ_3 plane). (2) The second explanation (shown in Fig. 7) relates the elongation component to a plane strain deformation model in a thrust ramp system. In this case, the pure shear component is a result of the ramp geometry on the deformation in the décollement level. Thus, deformation analysis of evaporitic rocks from décollements is a very useful means of understanding the kinematics of thrust belts and nappe emplacement. Indeed, numerous décollements of various ages and tectonic contexts localize in low strength evaporitic layers. This is particularly clear in the external zones of the Alpine chain where most of the tectonic contacts are outlined by Triassic evaporitic rocks, and several observations in different areas suggest that similar deformation structures and mechanisms occurred.

Acknowledgements—This work has been financed by the UA266 CNRS. Thanks are due to M. Mattauer and H. Philip who initiated this work and guided us to the study sites. We are grateful to A. Taboada for his help and for his enthusiastic discussions on deformation, and to J. P. Platt for fruitful improvements of the paper.

REFERENCES

Bulard, P. F., Chamagne, B., Darbeau, G., Delteil, J., Gioan, P., Ivaldi, J. P., Laval, F., Perez, J. L. & Polveche, J. 1975. Sur la genèse et les structures de l'arc de Nice. *Bull. Soc. géol. Fr.* **17**, 939–944.

Choukroune, P. 1971. Contribution à l'étude des mécanismes de la déformation avec schistosité grâce aux cristallisations syncinématiques dans les "zones abritées" ("pressure shadows"). *Bull. Soc. géol. Fr.* **13**, 257–271.

Cobbold, P. R., Gapais, D., Means, W. D. & Treagus, S. H. (editors). 1987. *Shear Criteria in Rocks. J. Struct. Geol.* **9**, 521–778.

Debelmas, J. 1979. Alpes: Savoie et Dauphiné. Guides Géologiques Régionaux, Masson.

Etchecopar, A. & Malavieille, J. 1987. Computer models of pressure shadows: a method for strain measurement and shear-sense determination. *J. Struct. Geol.* **9**, 667–677.

Fallot, P. 1949. Les chevauchements intercutanés de Roya (A.M.). *Ann. Hébert Haug. Lab. Géol. Fac. Sci. Univ. Paris* **7**, 161–170.

Fallot, P. & Faure-Muret, A. 1949. Sur l'extension du décollement de la série de couverture subalpine. *C. r. Acad. Sci., Paris* **228**, 616–619.

Gèze, B. 1960. La génèse néogène de l'arc de Nice (A.M.). *C. r. somm. Soc. Geol. Fr.* 33–34.

Gèze, B. 1963. Caractères structuraux de l'arc de Nice (A.M.). In: *Livre à la mémoire du Professeur P. Fallot. Mém. hors série Soc. géol. Fr.*, 289–300.

Gigot, P., Grandjacquet, C. & Haccard, D. 1974. Evolution tectonosédimentaire du bassin tertiaire de Digne depuis l'Eocène. *Bull. Soc. géol. Fr.* **16**, 128–139.

Ginsburg, L. 1959. Etude géologique de la bordure subalpine, à l'Ouest de la basse vallée du Var. *Bull. Serv. Carte géol. Fr.* **57** (2), 1–38.

Goguel, J. 1936. Description tectonique de la bordure des Alpes de la Bléone au Var. *Mém. Serv. Carte géol. Fr.*

Graham, R. H. 1981. Gravity sliding in the Maritime Alps. In: *Thrust and Nappe Tectonics* (edited by McClay, K. R. & Price, N. J.). *Spec. Publs geol. Soc. Lond.* **9**, 335–352.

Hugon, H. 1982. Structure et déformation du massif de Rocroi. Ardennes. Approche géométrique quantitative et expérimentale. Unpublished thèse 3ème cycle. Université de Rennes. France.

Larroque, J. M. & Ansart, M. 1985. Les déformations liées à la tectonique distensive du bassin potassique de Mulhouse: cas du secteur minier. *Bull. Soc. géol. Fr.* **1**, 837–847.

Lemoine, M., 1972. Rythme et modalités des glissements superposés dans les chaînes subalpines méridionales des Alpes occidentales françaises. *Geol. Rdsch.* **61**, 975–1010.

Malavieille, J. 1984. Modélisation expérimentale des chevauchements imbriqués: application aux chaînes de Montagnes. *Bull. Soc. géol. Fr.* **26**, 129–138.

Malavieille, J., Etchecopar, A. & Burg, J.-P. 1982. Analyse de la géométrie des zones abritées: simulation et application à des exemples naturels. *C. r. Acad. Sci., Paris* **294**, 279–284.

Marcoux, J., Brun, J.-P., Burg, J.-P. & Ricou, L. E. 1987. Shear structures in anhydrite at the base of thrust sheets (Antalya, Southern Turkey). *J. Struct. Geol.* **9**, 555–561.

Platt, J. P. & Vissers, P. L. M. 1980. Extensional structures in anisotropic rocks. *J. Struct. Geol.* **2**, 397–410.

Quinquis, H., Audren, C., Brun, J. P. & Cobbold, P. R. 1978. Intense progressive shear in Ile de Groix blueschists and compatibility with subduction or obduction. *Nature, Lond.* **273**, 43–45.

Ramay, J. G. & Huber, M. I. 1983. *The Techniques of Modern Structural Geology*, Vol. 1: *Strain Analysis*. Academic Press, New York.

Talbot, C. J. 1979. Fold train in a glacier of salt in southern Iran. *J. Struct. Geol.* **1**, 5–18.

Underhill, J. R. 1988. Triassic evaporites and Plio-Quaternary diapirism in western Greece. *J. geol. Soc. Lond.* **145**, 269–282.

Zack, I. & Freund, R. 1980. Strain measurements in eastern marginal shear zones of Mount Sedom Salt Diapir, Israel. *Bull. Am. Ass. Petrol. Geol.* **64**, 568–581.